4 Electronic Structure of Condensed Matter

4-1 Oscillations of Surface Magnetization in Fe/Ni/Cu(100) Films Observed with the Depth-resolved X-ray Magnetic Circular Dichroism Technique

Ultrathin Fe films on Cu(100) have attracted much interest due to their characteristic magnetic depth profiles. It has been believed that the two surface layers are ferromagnetically coupled, while the inner layers are in antiferromagnetic or spin-density-wave states below ~200 K. Recently, we have directly confirmed this magnetic structure by using a newly-developed technique, depth-resolved XMCD, in which the probing depth of the electron-yield XMCD spectrum is controlled by the electron detection angle [1].

If an Fe film is grown on a ferromagnetic substrate, the interface (bottom) layer interacts with the substrate, and one can expect some magnetic coupling between the surface and the interface via the inner layers. We have studied the surface and interface magnetic structure of Fe films grown on a Ni/Cu(100) film with the depth-resolved XMCD technique [2,3].

All the experiments described here were performed at BL-7A in an ultrahigh-vacuum chamber. Fe and Ni were deposited on a clean and ordered Cu(100) single crystal at room temperature. The sample was magnetized by a current pulse through a coil, and the coil was retracted during the measurement. The remanent magnetization was then investigated. A series of XMCD spectra with different probing depths were simultaneously recorded (see Fig. 1) in the partial electron yield mode with a retarding voltage of 500 V. All the spectra were recorded at grazing X-ray incidence, since the present films exhibited in-plane magnetization in the remanent state.

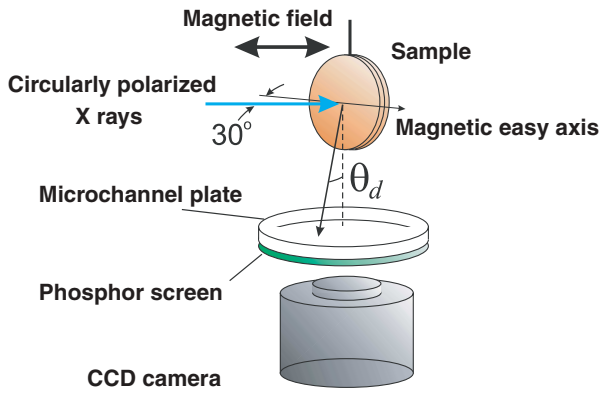

Figure 1
Schematic layout of the depth-resolved XMCD measurement. A set of electron yield XMCD spectra are recorded at different detection angles, θ_d, which correspond to different probing depths.

Series of XMCD spectra from Fe(4-9 ML)/Ni(6 ML)/Cu(100) films are given in Fig. 2(a) as a function of probing depth, λ_e. The spectra from the 4-ML Fe film are identical, irrespective of λ_e, indicating a uniform ferromagnetic structure. In contrast, the XMCD intensity from the 4.5-ML film drastically decreases with increasing λ_e. Moreover, the XMCD signal is opposite in sign to that from the 4-ML film. These results show that the surface of the 4.5-ML film has a magnetization opposite to the applied field, and that its magnitude is larger than that of the inner layers. As the Fe thickness further increases, the XMCD signal almost vanishes at 6 ML, and reappears with opposite sign at 9 ML. The Ni film exhibited a positive magnetization independent of the Fe thickness (spectra not shown).

The obtained data were analyzed assuming that the Fe film consists of three regions; two surface layers, a single interface (bottom) layer, and the remaining inner layers [3]. The estimated surface and interface magnetizations are depicted in Fig. 2(b) as a function of Fe thickness. The surface magnetization shows oscillatory behavior, while the interface one stays almost unchanged. The inner layers were found to be almost nonmagnetic (< 0.2 μ_B, not shown). Note here that the observed oscillation in the surface magnetization can be also interpreted as a rotation of the magnetic moment. If the surface magnetic moment rotates as a function of Fe thickness, there should be two equivalent domains in which the moment rotates in clockwise and counterclockwise directions. Therefore, the resultant magnetization should oscillate due to the averaging over the two domains. An oscilla-

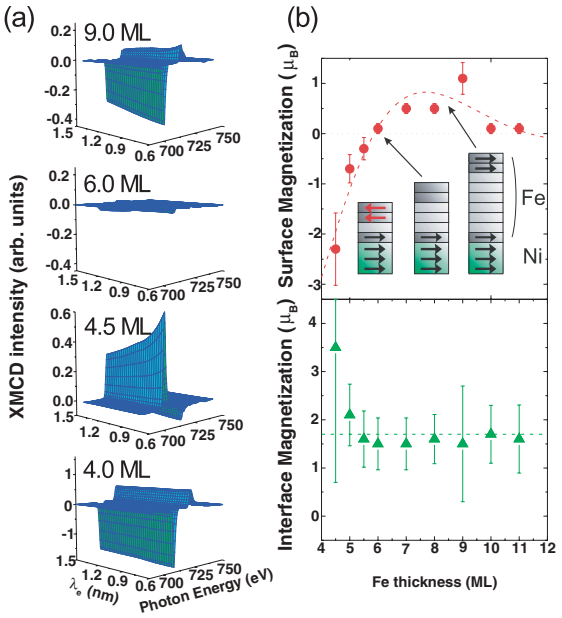

Figure 2
(a) Fe L-edge XMCD spectra from Fe(4-9 ML)/Ni(6 ML)/Cu(100) films with different probing depths, λ_e, recorded at 200 K. (b) Estimated surface and interface magnetization, together with the deduced magnetic structure model.

tory or rotational magnetic interaction is thus suggested between the surface and interface via the nonmagnetic inner layers.

References

[1] K. Amemiya, S. Kitagawa, D. Matsumura, H. Abe, T. Ohta and T. Yokoyama, *Appl. Phys. Lett.*, **84** (2004) 936.

[2] K. Amemiya, D. Matsumura, H. Abe, S. Kitagawa, T. Ohta and T. Yokoyama, *Phys. Rev. B,* **70** (2004) 195405.

[3] K. Amemiya, D. Matsumura, H. Abe, S. Kitagawa, T. Yokoyama and T. Ohta, *J. Electron Spectrosc. Relat. Phenom.*, **144** (2005) 689.

K. Amemiya[1], D. Matsumura[1], H. Abe[1], S. Kitagawa[1], T. Yokoayma[2] and T. Ohta[1] ([1]Univ. of Tokyo, [2]IMS)

4-2 Combinatorial *in situ* Photoemission Spectroscopy of Strongly Correlated Oxide Heterointerfaces

Superlattices based on perovskite transition-metal oxides have attracted much attention because of the possibility of tuning the magnetic and electronic properties of a thin film in a way that would not be possible in single-phase bulk materials [1-3]. Extensive studies on the behavior of perovskite-based superlattices have demonstrated that the magnetic and electronic properties of oxides can be controlled or modified through interface effects, such as spin exchange interactions, charge transfer, and epitaxial strain. However, the lack of information on the electronic structure of the interfacial layers, in particular the occurrence of charge transfer between constituent layers, prevents us from fabricating superlattices with the desired properties. To design devices which use perovskite oxides, it is critically important to understand the electronic structure of oxide heterointerfaces.

$La_{0.6}Sr_{0.4}FeO_3$ (LSFO)/$L_{0.6}Sr_{0.4}MnO_3$ (LSMO) superlattices have attracted great attention since they show an unusually enhanced magnetoresistance [3]. For the interface electronic structure analysis of these superlattices, we have employed an *in situ* photoemission spectroscopy system combined with a combinatorial laser molecular beam epitaxy (laser MBE) thin film growth system at BL-2C [4]. Using these systems, we have determined the compositional change in the electronic structures of LSFO/LSMO multilayers. We fabricated combinatorial libraries in the laser MBE chamber. A schematic side view of the combinatorial libraries is shown in the inset of Fig. 3. For precisely determining the interfacial electronic structure, we performed Mn 2p-3d resonant photoemission (RPES) measurements at BL-2C. The strong enhancement of Mn 3d states at Mn 2p-3d threshold enables us to extract the true Mn 3d partial density of states (PDOS) of the LSMO layers in the vicinity of the interface with the LSFO overlayer.

The obtained Mn 3d PDOS for the LSMO layer at the abrupt LSFO/LSMO interfaces are shown in Fig. 3 [5]. Using the RPES technique, it is possible to investigate the Mn 3d PDOS of LSMO layers buried in LSFO overlayers. The Mn 3d spectra consist of two prominent peaks at about 2.1 and 0.8 eV. These peaks are assigned to the Mn 3d $t_{2g}\uparrow$ and $e_g\uparrow$ states [6]. The spectra in Fig. 3 show an interesting change in spectral intensity near E_F, reflecting the modulated electronic structure at the interface; the intensity of the $e_g\uparrow$ states drops dramatically as the LSFO overlayer thickness increases, while the $t_{2g}\uparrow$ states show no noticeable change. Similar changes in the peak intensities of the $e_g\uparrow$ states have been observed in $La_{1-x}Sr_xMnO_3$ as a function of carrier concentrations [6]. The reduction of the spectral intensity of the $e_g\uparrow$ states with increasing LSFO overlayer thickness therefore clearly indicates the occurrence of electron transfer from LSMO to LSFO layers in the interface region.

Since the LSFO and LSMO layers share a common A-site composition ($La_{0.6}Sr_{0.4}$), the MnO_2 and FeO_2 atomic layers are not subjected to a chemical modulation of carrier concentration at the interface [3,5]. The behavior of the system can be explained by considering the electronic structure of Fe and Mn, as illustrated in Fig. 4. Owing to the energy difference of the partially occupied $e_g\uparrow$ states of the Fe and Mn ions, it is clear that electrons can be transferred from the $e_g\uparrow$ states of LSMO into the corresponding states in LSFO, resulting in an effective increase of hole concentration in the LSMO layers close to the LSFO interface. These results show that an intrinsic "dead layer" exists at the LSFO/LSMO interface due to the interfacial charge transfer between the 3d levels of the constituent transition metals.

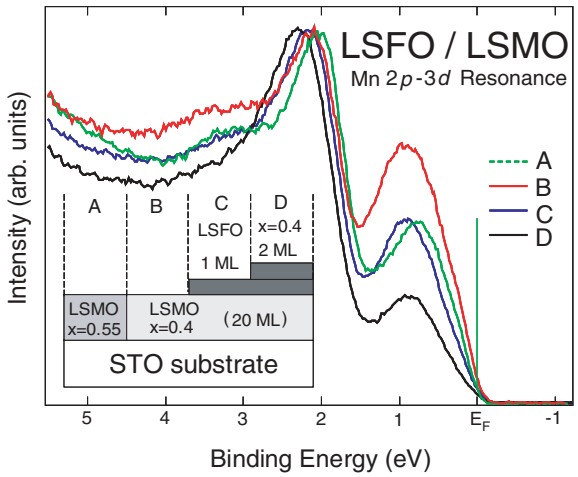

Figure 3
Mn 3d spectra of LSMO layers in the vicinity of an interface with LSFO. Mn 3d spectra of LSMO (x = 0.4(B) and 0.55(A)) films are also presented for comparison. The inset shows schematic side views of the measured libraries A-D.

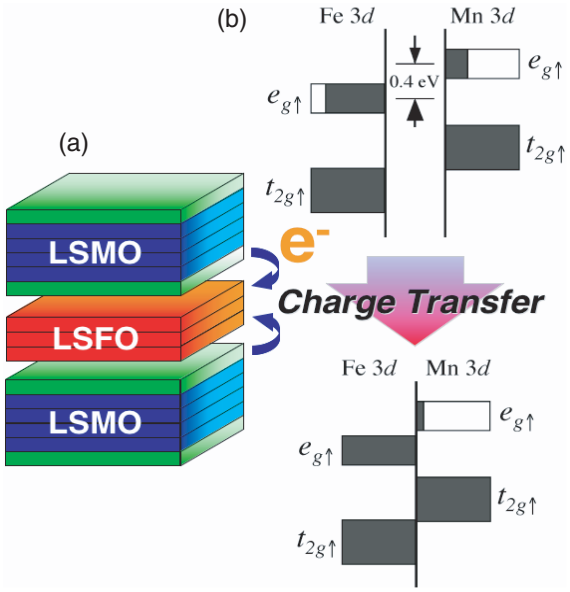

Figure 4
A schematic diagram of the electronic structure of Fe and Mn ions for (a) LSFO and LSMO films and (b) the LSFO/LSMO interface. Electrons are transferred from the Mn 3d $e_g\uparrow$ to the Fe 3d $e_g\uparrow$ states across the interface. As a result of the charge transfer, a magnetic "dead layer" is formed at the heterointerface.

M. Oshima and H. Kumigashira (The Univ. of Tokyo)

References

[1] K. Ueda, H. Tabata and T. Kawai, *Science,* **280** (1998) 1064.
[2] H. Yamada, Y. Ogawa, Y. Ishii, H. Sato, M. Kawasaki, H. Akoh and Y. Tokura, *Science,* **305** (2004) 646.
[3] M. Izumi, Y. Murakami, Y. Konishi, T. Manako, M. Kawasaki and Y. Tokura, *Phys. Rev. B,* **60** (1999) 1211.
[4] K. Horiba, H. Ohguchi, H. Kumigashira, M. Oshima, K. Ono, N. Nakagawa, M. Lippmaa, M. Kawasaki and H. Koinuma, *Rev. Sci. Instrum.*, **74** (2003) 3406.
[5] H. Kumigashira, D. Kobayashi, R. Hashimoto, A. Chikamatsu, M. Oshima, N. Nakagawa, T. Ohnishi, M. Lippmaa, H. Wadati, A. Fujimori, K. Ono, M. Kawasaki and H. Koinuma, *Appl. Phys. Lett.*, **84** (2004) 5353.
[6] K. Horiba, A. Chikamatsu, H. Kumigashira, M. Oshima, N. Nakagawa, M. Lippmaa, K. Ono, M. Kawasaki and H. Koinuma, *Phys. Rev. B,* **71** (2005) 155420.

4-3 Antiferromagnetic Domain Imaging of NiO(100) by PEEM, and the Non-magnetic Linear Dichroism Effect at the O *K* Edge

NiO is known to be a typical antiferromagnetic (AFM) material (it has a Néel temperature T_N=523 K). Below T_N, its crystal structure is slightly deformed along one of the four <111> axes with a rhombohedral contraction from the original cubic rocksalt structure. Crystallographic twinning due to the contraction leads to four different possible domains, the so-called *T(win)*-domains, with different contraction <111> axes. Each *T*-domain has an easy axis along one of three [211]-derived directions and is split into three different *S(pin)*-domains. Photoelectron emission microscopy (PEEM) with synchrotron radiation (SR-PEEM), combined with magnetic linear dichroism studies (MLD) at the Ni L_2 edge has recently come to be used for the study of the AFM domain structure of cleaved NiO(100) surfaces [1].

At BL-2C, 11A and 13C, we have observed similar AFM domains of NiO(100) with SR-PEEM using linearly polarized light but near the O *K* edge [2]. This result was unexpected and unordinary, because the O atom should not have any magnetic moment. It is supposed that the origin of the unexpected LD is the strong interaction between the O 2*p* components and the Ni 3*d* components. However, it is not clear whether the crystal distortion effect is essential to the non-magnetic LD or not. In order to confirm this, we have investigated the effect after deposition of magnetic metal films on to the substrate.

Fig. 5(a) shows the domain structure for the Fe(wedge)/NiO system obtained at the Ni L_2 edge in the 3~5 ML deposition region. In the same manner, the domain structure obtained for the same surface but at the O *K* edge is shown in Fig. 5(b). In Figs. 5(c) and 5(d), the same images but for the ~10 ML region are shown. In the lower coverage region shown in (a) and (b), the domain patterns are similar, reflecting mainly the AFM domain structures of the NiO substrate. However, in the higher coverage region shown in (c) and (d), the domain pattern obtained at the Ni L_2 edge (c) is strongly affected and has almost disappeared compared to the clear image obtained at the O *K* edge (d). If the twinned structure of the crystal is essential for the observation of the domain at the O *K* edge, the observed image should not be affected by the deposition because the distortion can not be strongly affected by the deposition. In contrast, the observed domain image at the Ni L_2 edge may easily be affected by metal deposition. Therefore, this phenomenon demonstrates evidence that the AFM domain structure observed at the O *K* edge reflects the *T*-domain and that

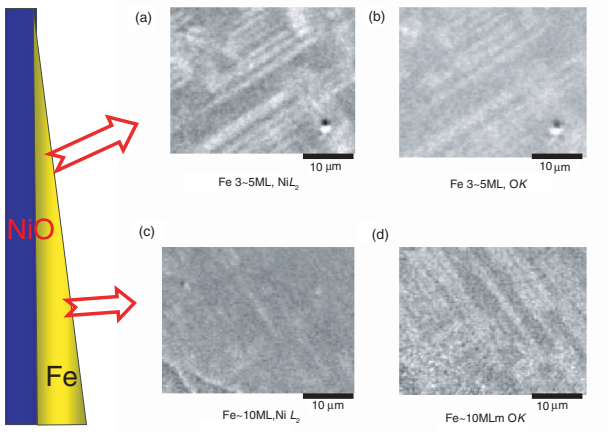

Figure 5
AFM domain images of wedge-shaped Fe covered surfaces of NiO(100). (a) Image at the Fe 3~5 ML region observed at the Ni L_2 edge. The ratio of two images recorded at 870.2 eV and 871.5 eV is taken in order to obtain a clear AFM domain contrast. (b) Same as in (a) but at the O *K* edge (528.3 eV and 537.0 eV). (c) Same as in (a) but at the Fe ~10 ML region. (d) Same as in (c), but at the O *K* edge.

the crystal distortion effect is essential for understanding the observed image. Probably due to the exchange coupling effect at the interface, the *S*-domain is strongly affected whereas the *T*-domain is affected only weakly.

T. Kinoshita[1, 2], T. Wakita[2], H. -L. Sun[1], T. Tohyama[3], A. Harasawa[1], H. Kiwata[1], K. Ono[4], T. Matsushima[1], M. Oshima[1], N. Ueno[3], T. Okuda[1] ([1]Univ. Tokyo, [2] JASRI/SPring-8, [3]Chiba Univ., [4]KEK-PF)

References

[1] H. Ohldag, A. Scholl, F. Nolting, S. Anders, F. U. Hillebrecht and J. Stöhr, *Phys. Rev. Lett.*, **86** (2001) 2878.

[2] T. Kinoshita, T. Wakita, H. -L. Sun, T. Tohyama, A. Harasawa, H. Kiwata, F. U. Hillebrecht, K. Ono, T. Matsushima, M. Oshima, N. Ueno, Y. Saitoh and T. Okuda, *J. Phys. Soc. Jpn.*, **73** (2004) 2932.

4-4 Indication of Room-temperature Ferromagnetism Induced by Doped Co Ions in $Ti_{1-x}Co_xO_{2-\delta}$: An X-ray Magnetic Circular Dichroism Study

Dilute magnetic semiconductors (DMS) have attracted much scientific and technological interest because they are thought to be promising materials for spintronic devices. Since the discovery of room-temperature ferromagnetism in Co-doped anatase- and rutile-type TiO_2 [1, 2], oxide magnetic semiconductors have been intensively studied. Although many ferromagnetic oxide DMSs have been reported, the origin of ferromagnetism in these materials remains controversial. An X-ray magnetic circular dichroism (XMCD) study has recently been reported on Co-doped anatase-type TiO_2, but the results showed that the ferromagnetism arises extrinsically from segregated Co clusters after heat treatment [3]. Thus, it is still an open question whether the ferromagnetism originates from the intrinsic character of the materials or from segregated nano-scale magnetic impurities.

We have studied the origin of the reported ferromagnetism in Co-doped rutile-type TiO_2 [2] by making high-precision XMCD measurements at the Co $L_{3,2}$ edges on carefully prepared samples. The samples were grown on r-sapphire ($10\bar{1}2$) substrates at 400ºC under an oxygen pressure of 1×10^{-7} Torr using the PLD method. Ferromagnetism was confirmed at room temperature by both the anomalous Hall effect and by magnetization measurements with a SQUID magnetometer [4].

Fig. 6 shows the Co L_3-edge X-ray absorption spectrum (XAS) and XMCD spectrum of the rutile-type $Ti_{0.97}Co_{0.03}O_{2-\delta}$ film. The spectra were recorded at room temperature with the total electron-yield method using circularly polarized soft X-rays at BL-11A and AR-NE1B. Magnetic fields of ±1 T were applied to the as-deposited sample with neither Ar ion sputtering nor annealing. The XMCD spectrum of metallic Co (reduced in amplitude to 0.06 scale) is also shown in Fig. 6 for comparison. The XAS spectrum shows multiplet features, denoted in Fig. 6(a) by arrows A to E. Multiplet features were also observed in the XMCD spectrum, corresponding to those in the XAS. What is the most remarkable in the XMCD spectrum is a clear negative peak corresponding to peak D in the XAS. No corresponding feature was seen in the XMCD spectrum of metallic Co. The dominant negative peak in the XMCD spectrum exhibits a line shape more flattened than that in the XMCD spectrum of metallic Co, indicating overlapping, unresolved multiplet features corresponding to features B and C in the XAS spectrum. A positive peak was observed in the XMCD spectrum, corresponding to feature A in the XAS spectrum. The XMCD spectrum at the Co L_2 edge shows doublet features corresponding to a peak and a shoulder in the XAS. The present observation of multiplet features in the XMCD spectrum strongly indicates that the ferromagnetism originates from Co ions with localized *d* electrons, in sharp contrast to the result of a previous XMCD study [3].

Fig. 7 shows a comparison of the experimental XMCD spectrum with the results of full atomic multiplet calcula-

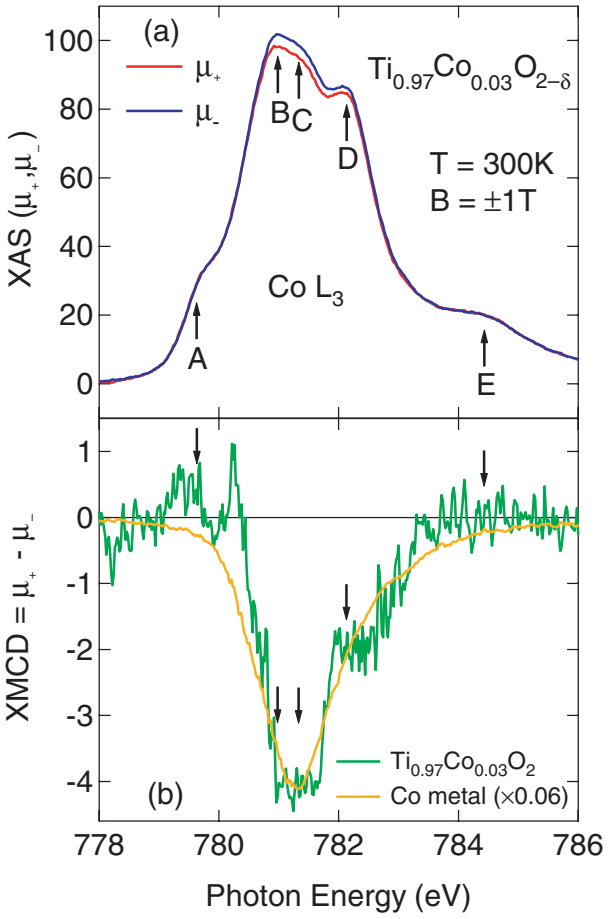

Figure 6
(a) Photon-helicity dependent Co L_3 X-ray absorption spectra (XAS) of rutile-type $Ti_{0.97}Co_{0.03}O_{2-\delta}$($\mu_+$: red curve, μ_- : blue curve). (b) Co L_3 X-ray magnetic circular dichroism (XMCD) of rutile-type $Ti_{0.97}Co_{0.03}O_{2-\delta}$ (green curve). The XMCD spectrum of metallic Co is also plotted with 0.06 scaling (orange curve).

tions. The calculations have been made for a low-spin Co^{2+} ion in the crystal field with O_h symmetry, a high-spin Co^{2+} ion in the crystal field with O_h symmetry, and a high-spin Co^{2+} ion in the crystal field with D_{2h} symmetry. The possibility of the Co^{2+} low-spin state in O_h symmetry is immediately ruled out. The experimental XMCD spectrum shows qualitatively the best agreement with the calculated spectrum for the Co^{2+} high-spin configuration in D_{2h} symmetry. These results verify the intrinsic ferromagnetism induced by the high-spin Co^{2+} ions substituting the Ti^{4+} ions in $Ti_{0.97}Co_{0.03}O_{2-\delta}$.

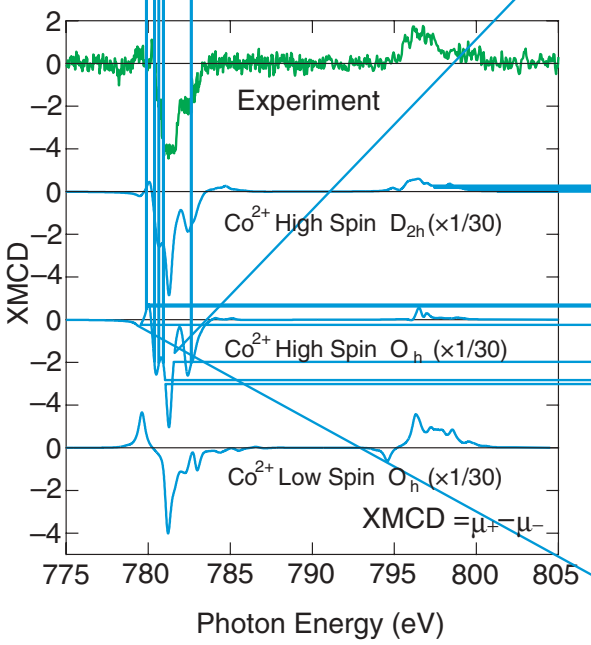

Figure 7
Comparison of the experimental XMCD (green curve) with atomic multiplet calculations (light blue curves). Calculations were done for the low-spin Co^{2+} ion and the high-spin Co^{2+} ion in the crystal field with O_h symmetry, and the high-spin Co^{2+} ion in the crystal field with D_{2h} symmetry. The calculated XMCD spectra have been scaled by a factor of 1/30 for comparison with the experimental XMCD spectrum.

K. Mamiya[1], A. Fujimori[2], T. Koide[1], H. Tokano[3], H. Manaka[4], A. Tanaka[5], H. Toyosaki[6], T. Fukumura[6], and M. Kawasaki[6,7] ([1]KEK-PF, [2]Univ. of Tokyo, [3]Univ. of Tsukuba, [4]Kagoshima Univ., [5]Hiroshima Univ., [6]Tohoku Univ., [7]NIMS)

References

[1] Y. Matsumoto, M. Murakami, T. Shono, T. Hasegawa, T. Fukumura, M. Kawasaki, P. Ahmet, T. Chikyow, S. Koshihara, H. Koinuma, *Science,* **291** (2001) 854.
[2] Y. Matsumoto, R. Takahashi, M. Murakami, T. Koida, X. -J. Fan, T. Hasegawa, T. Fukumura, M. Kawasaki, S. -Y. Koshihara, and H. Koinuma, *Jpn. J. Appl. Phys.*, **40** (2001) L1204.
[3] J. -Y. Kim, J. -H. Park, B. -G. Park, H. -J. Noh, S. -J. Oh, J. S. Yang, D. -H. Kim, S. D. Bu, T. -W. Noh, H. -J. Lin, H. -H. Hsieh, and C. T. Chen, *Phys. Rev. Lett.*, **90** (2003) 017401.
[4] H. Toyosaki, T. Fukumura, Y. Yamada, K. Nakajima, T. Chikyow, T. Hasegawa, H. Koinuma and M. Kawasaki, *Nature Materials,* **3** (2004) 221.

4-5 Evaluation of Diffusion Barrier Continuity on Porous Low-k Films Using Positronium Time of Flight Spectroscopy

Bose-Einstein condensation (BEC) effects in many positronium atoms (Ps) would be interesting to observe in a material in which there are a great many interconnected pores, such that Ps can diffuse over long distances. For the purpose of the production of a dense Ps gas, the diffusion barrier must be continuous and very thin, and the tradeoff between continuity and thickness of the barrier affects the Ps gas density in the porous layer underneath. In the present work, a depth-profiled positron time of flight (Ps-TOF) experiment was performed to investigate a diffusion barrier on a spin-on low dielectric constant (low-k) porous silica film. We studied a capping layer of 50-nm amorphous SiO_2, which was optimized for 3-keV positron (e^+) penetration through the capping and stopping in the porous layer. Maximum positronium intensity was found with positron implantation energy of 3 keV that reflects the sample structure is consistent with an open pore fraction $\eta < 2 \cdot 10^{-4}$ of the capping layer.

Fig. 8(A) shows the positron implantation energy dependence of the Ps-TOF spectrum for various positron impact energies and Fig. 8(B) the integrated Ps decay events over the time region 95 ns –100 ns. The variations in Ps yield reflect the sample structure. At an impact energy of 0.5 keV, surface Ps escapes, and leads to the small bump at about 100 ns time of flight. At 1 keV the

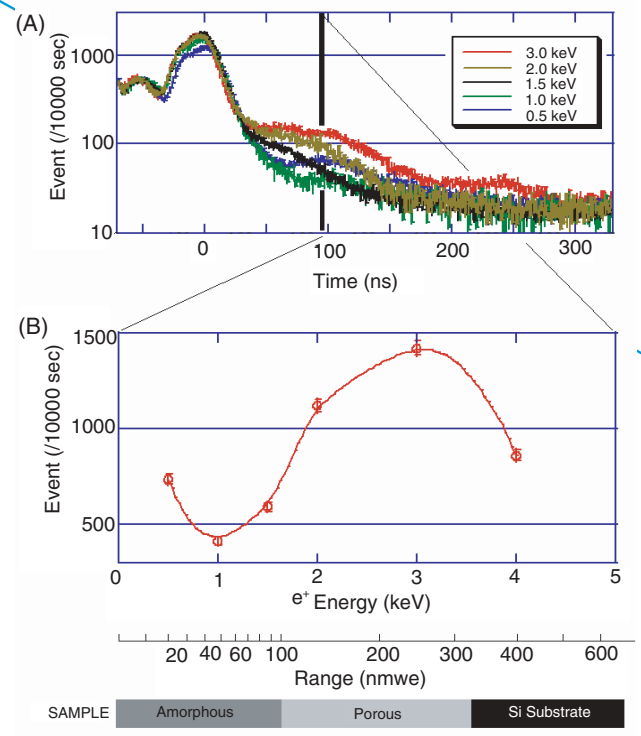

Figure 8
(A)Ps-TOF spectra at various positron energies for the present sample. (B) Integrated decay events over t = 95-100 ns versus positron energy. Here, a term, nmwe, represents a nanometer water equivalent.

positrons are stopped in the a-silica from which little Ps escapes due to its short diffusion length and short lifetime. At 3 keV, Ps forms copiously in the porous layer, thermalizes and escapes through cracks or other gaps in the capping layer. Finally at 4 keV the delayed Ps time of flight bump is attenuated because positrons are being lost to the solid substrate. We note that the cracks in the capping layer do not themselves lead to significant Ps emission at 1 keV because the crack density is very low compared to the inverse of the positronium diffusion length which is rather short (~100 nm) in the cap layer.

The authors are grateful to Y. Yan and Z. Li, E. L. Chronister, M. McIntire, D. Cassidy, R. Castillo and K. Nagamine. This work was supported in part by a JSPS Core to Core Program. We are also grateful for financial support from the University of California Institute for Mexico and the United States (UC MEXUS).

H. K. M. Tanaka[1,2], T. Kurihara[3] and A. P. Mills Jr.[1]
([1]UC-Riverside, [2]KEK-Muon, [3]KEK-PF)